Energy spectrum and the Shubnikov-de Haas effect in acceptor-type graphite heterointercalaction compounds

V. V. Avdeev, V. Ya Akim, N. B. Brandt, V. N. Davydov, V. A. Kulbachinskii, and S. G. Ionov

M. V. Lomonosov Moscow State University
(Submitted 19 October 1987)
Zh. Eksp. Teor. Fiz. **94**, 188–201 (December 1988)

A new class of interstitial graphite compounds (IGCs)—heterointercalated IGCs—has been synthesized. In each of these a layer of graphite and a layer of intercalate alternate rigorously. The electrophysical properties of the first-stage acceptor-type heterointercalated IGCs $C_{10}CuCl_2 \cdot 0.6$ ICl and $C_{15}CuCl_2 \cdot 1.2$ ICl have been investigated in the temperature range 1.6–300 K in magnetic fields $B \leqslant 10$ T. Several distinct frequencies are observed in Shubnikov–de Haas (ShdH) measurements in these compounds, in contrast to the single frequency observed in the usual first-stage IGCs. This indicates the complexity of the energy spectrum in the heterointercalates. The Fermi surface cross-sectional area and carrier effective mass have been determined, as well as their variation under pressure. A model of the energy spectrum of the hetero-IGCs is proposed, based on the graphite spectrum and taking into account dispersion of charge carriers along the c axis.

INTRODUCTION

The widespread interest in study of one class of compounds with a two-dimensional structure—the synthetic metals based on IGCs—was stimulated by both the high conductivity and low specific weight of these compounds and the possibility of studying charge transport in quasi-two-dimensional structures. There now exists a whole class of substances which, if introduced separately into a graphite matrix, can result in completely monocrystalline IGCs of different stages, beginning with the first[1] (the stage number N is determined by the number of graphite layers between two nearest-neighbor layers of intercalated material). The high degree of perfection of the IGCs presently produced allows one to use quantum oscillatory effects to study their energy spectrum and derive information on the shape and dimensions of the Fermi surface, concentrations of charge carriers and effective masses.

The effectiveness of the intercalates differs; that is the number of charge carriers in the graphite layers is increased to a different degree depending on the substance chosen to introduce. When halogens, interhalides, metal halides, or acids are intercalated, acceptor-type IGCs are produced; that is, the majority carriers in the substance are holes. The hole concentration and the conductivity of acceptor IGCs usually grow when a stronger oxidant is used, but only up to a certain limit. If a very strong oxidant is used bonds are formed between carbon atoms and the oxidant, and the hole concentration falls. Up to the present there is no single point of view on the origin of the IGC energy spectrum and the reason for their high conductivity in the basal plane.

New possibilities for the understanding of the physical properties of the IGCs are opened by a complex intercalation in which there are sequential layers of graphite, an intercalate 1, and an intercalate 2. Such compounds, referred to as heterointercalated,[2,3] can be divided into two classes: those with acceptor-acceptor and acceptor-donor intercalate sequences. In the first case, the volatile chlorides (AlC_3, $FeCl_3$, $GaCl_3$) are introduced into IGCs of the nonvolatile metal chlorides ($NiCl_2$, $CoCl_2$) with stage number $N \geqslant 2$; in the second case the alkali metals (K, Rb, Cs) are introduced into these IGCs.[2,4] We note that the samples in Refs. 2 and 4 are not single-phase, and there are no data on their electrophysical properties.

Here we report the results of a study on the Shubnikov-de Haas effect in the first synthesized hetero-IGCs (with a high degree of periodicity and two different intercalates) of the first-stage acceptor type. These were prepared using copper chloride ($CuCl_2$) as the first intercalate and iodine monochloride (ICl) as the second. The chemical formulas of the compounds investigated are $C_{10}CuCl_2 \cdot 0.6$ ICl and $C_{15}CuCl_2 \cdot 1.2$ ICl. A model is proposed for the energy spectrum of the low-stage, acceptor-type hetero-IGCs which agrees with the experimental data.

SYNTHESIS OF THE HETERO-ICGs

To synthesize the hetero-IGCs, highly ordered graphite of type UPV-1TMO was used. The angle of crystallite misorientation relative to the basal plane was less than 1°, and the crystallite dimension in the basal plane was 10^5 Å. Copper chloride (II) was produced by dehydration of the crystalline hydrate $CuCl_2 \cdot 2H_2O$ in boiling sulfur chloride with subsequent distillation of excess $SOCl_2$. Purification of the anhydrous copper chloride was carried out by distillation of the product in a stream of dry chlorine at $T = 950$ K. The iodine monochloride was produced by synthesis from the elements and purified by recrystallization from the melt.

The compounds $C_{10}CuCl_2 \cdot 0.6$ ICl and $C_{15}CuCl_2 \cdot 1.2$ ICl were synthesized in two stages. To begin, second-stage $C_{10}CuCl_2$ IGC and third-stage $C_{15}CuCl_2$ IGC were produced. Synthesis of the $C_{10}CuCl_2$ IGC was carried out over the course of two weeks by the gas-phase method in a two-section ampoule at a temperature of 610 C for the graphite and 600 C for the chloride. Synthesis of $C_{15}CuCl_2$ IGC was carried out in the same way, but with a graphite temperature of 650 C. According to x-ray analysis the intercalate layer thickness in the IGCs was 9.40 Å, and the repeat period along the C-axis was 12.75 Å for the second-stage IGC and 16.10 Å for the third-stage IGC. The samples produced had an excellent degree of regularity. The introduction of the iodine monochloride at 40 C resulted in the filling of all the
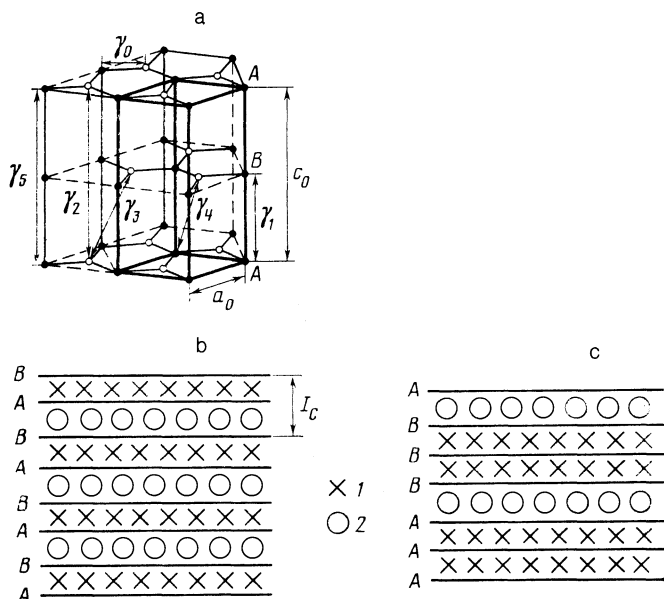
FIG. 1. Schematic representation of the structure of graphite and the hetero-IGCs: A and B are the distinct graphite layers, 1 is an ICl molecule, and 2 is a $CuCl_2$ molecule. (a) The graphite structure. Light and dark points are carbon atoms. (b) A possible structure for the hetero-IGC $C_{10}CuCl_2 \cdot 0.6$ ICl; I_C is the repeat period. (c) A possible structure for the IGC $C_{15}CuCl_2 \cdot 1.2$ ICl.

FIG. 2. Diffractograms of (a) the third-stage IGC $C_{15}CuCl_2$; (b) the hetero-IGC $C_{15}CuCl_2 \cdot 1.2$ ICl; and (c) the hetero-IGC $C_{10}CuCl_2 \cdot 0.6$ ICl. Numbers on the peak are reflection indices.

free interlayer spaces and the formation of a first-stage IGC with alternating layers of the different intercalates and graphite.

The graphite structure is shown in Fig. 1a, the proposed structure of the $C_{10}CuCl_2 \cdot 0.6$ ICl compound in Fig. 1b, and the possible graphite layer sequence in $C_{15}CuCl_2 \cdot 1.2$ ICl in Fig. 1c. The graphite layer sequence AA has been experimentally observed in acceptor-type IGCs (see, for example, Ref. 5). X-ray analysis with the Dron-2 diffractometer (Co K_α radiation, Fe absorber) showed that the samples were single-phase and had a repeat period of 16.56 Å for $C_{10}CuCl_2 \cdot 0.6$ ICl and of 23.70 Å for $C_{15}CuCl_2 \cdot 1.2$ ICl, with an uncertainty of 0.02 Å. The corresponding diffractograms are shown in Fig. 2. The widths of the intercalate layers in the second-stage mono-IGCs of $CuCl_2$ and ICl are equal to 9.40 Å and 7.12 Å, respectively. Based on this, we would expect repeat periods $I_{c1} = d_c^{CuCl2} + d_c^{ICl} = (9.40 + 7.12)$ Å $= 16.52$ Å and $I_c = (9.40 + 27.12)$ Å $= 23.64$ Å. The larger values in the IGCs synthesized can be interpreted as a consequence of the stronger electrostatic interaction of the charged intercalate complexes in neighboring layers of the first-stage hetero-IGCs compared to the second-stage mono-IGCs.

THE SHUBNIKOV–de HAAS EFFECT AND THE ENERGY SPECTRUM OF THE FIRST-STAGE HETERO-IGC $C_{10}CuCl_2 \cdot 0.6$ ICl

The room-temperature conductivity σ of the IGC $C_{10}CuCl_2 \cdot 0.6$ ICl is 2.5×10^5 ohm^{-1} cm^{-1} m, nearly twice as high as that in the first-stage monointercalated IGCs of the same materials. When the temperature is reduced to 4.2 K σ increases by a factor of 3 to 7; the larger the room-temperature σ, the stronger the increase upon cooling. The relatively small decrease in resistance at low temperatures, for a high (of the order of 10^4 cm^2/V·s) carrier mobility, is
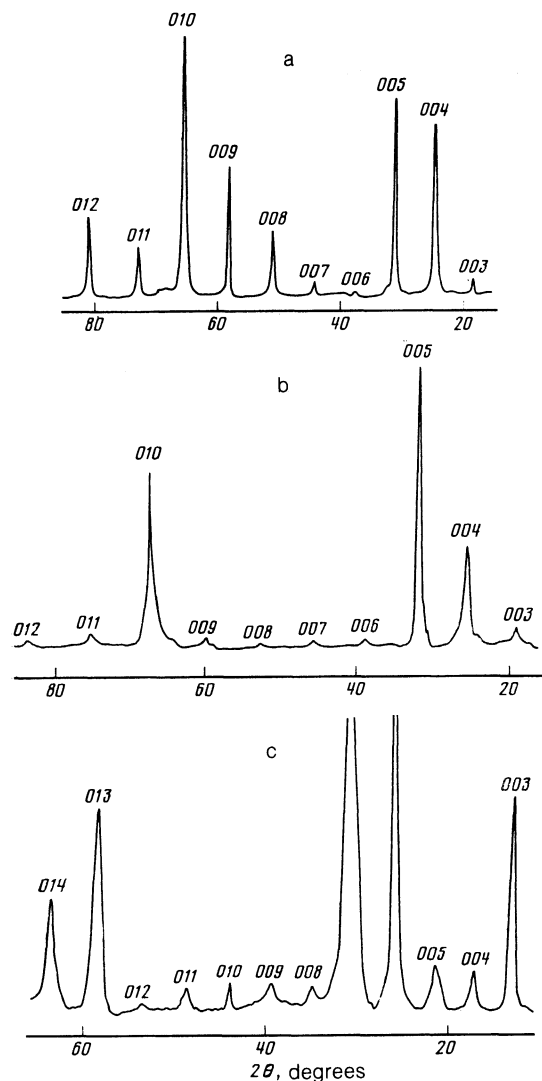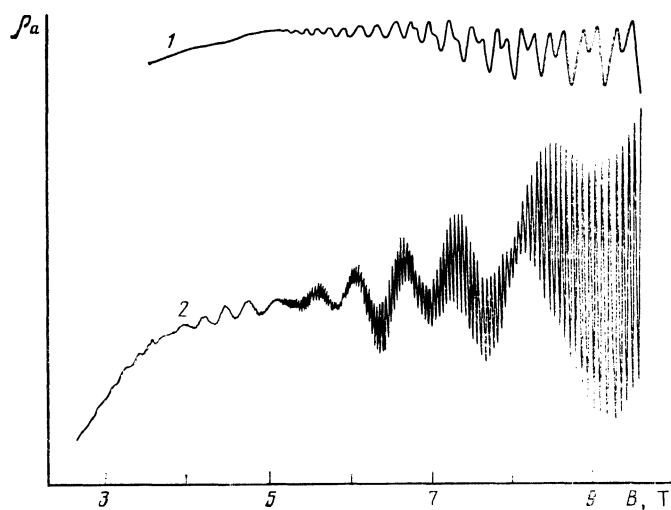

FIG. 3. Dependence of the oscillatory part of the transverse magnetoresistance ρ_a on magnetic field: 1—the second stage IGC $C_{10}CuCl_2$; 2—the first-stage IGC $C_{10}CuCl_2 \cdot 0.6$ ICl.

TABLE I. Parameters of investigated IGCs.

IGC composition	N	$S \cdot 10^{-12}$, cm^{-2}	m^*/m_0	ε_F, eV	γ_0, eV	γ_1, eV
$C_{10}CuCl_2$	2	164	0.09	-0.25	2.7	0.37
$C_{15}CuCl_2$	3	22 127 } 480 }	—	-0.54	3.0	0.37
$C_{10}CuCl_2 \cdot 0{,}6ICl$	1	54 (S_2^K) } 62 (S_2^H) } 1000 (S_1^H) } 1020 (S_1^K) }	0.10±0.01 0.38±0.05	-0.56	2.0	0.24
$C_{15}CuCl_2 \cdot 1{,}2ICl$	1	64–82 } 254–270 } 910–950 }	0.20±0.05	-0.69	2,4	0.28

Notation: S is the extremal Fermi-surface cross-section, m^* is the effective mass, and m_0 is the free-electron mass.

evidence of the weak electron-phonon interaction in this type of hetero-IGCs.

The change in the ShdH oscillations of the second-stage $C_{10}CuCl_2$ compound upon introduction of the iodine monochloride to form the first hetero-IGC $C_{10}CuCl_2 \cdot 0.6$ ICl is illustrated in Fig. 3. Compared to the original $C_{10}CuCl_2$ compound in which only one oscillation frequency is observed, the energy spectrum of the $C_{10}CuCl_2 \cdot 0.6$ ICl is much more complicated. The ShdH oscillations of the first-stage compound are a superposition of two frequencies. In both the lower and higher frequencies beats are seen, evidence of two close frequencies of different amplitude in each harmonic. The corresponding extremal Fermi-surface cross-sections are $S_1^K = 1020$, $S_1^H = 1000$, $S_2^K = 54$ and $S_2^H = 62$ in units of 10^{12} cm^{-2}. The Dingell temperature T_D for the parent graphite is 8 K; in the hetero-IGC, T_D grows to $\simeq 13$–15 K.

Thus, the two-stage synthesis carried out causes an insignificant rise in the Dingell temperature and leaves practically unchanged the magnetic field value at which oscillations set in. Since these values depend on the mean-free path length of the carriers, these results prove that the additional intercalation does not substantially affect their scattering dynamics. Effective masses for the carriers, averaged over the maximum and minimum cross-sectional area of each Fermi-surface cylinder, are shown in Table I.

The appearance of several ShdH frequencies in the first-stage IGC $C_{10}CuCl_2 \cdot 0.6$ ICl (see Fig. 3) was unexpected. It is usually assumed that the energy spectrum of the first-stage intercalated compounds is described by the two-dimensional Blinowski model.[6] In this model it is assumed that acceptor IGCs do not have translational symmetry in view of the lack of correlation of intercalate distribution from layer to layer. The lack of translational symmetry necessarily leads to a two-dimensional description of the electronic band structure of the acceptor IGCs. This assumption allows one to carry out a tight-binding calculation and to plot an energy spectrum corresponding to a single cylindrical isoenergetic surface for first-stage IGCs. On the basis of this one can satisfactorily describe the near-infrared optical properties of these IGCs. Therefore, observations of several oscillation frequencies in the first-stage hetero-IGCs has fundamental significance and requires detailed discussion.

One reason for the appearance of several frequencies in the ShdH effect along with preservation of the two-dimensional character of transport may be the formation of an ICl

superlattice commensurate with the graphite lattice. This has been observed in IGCs of iodine monochloride[7] and of antimony pentachloride.[8,9] However, experiments in which samples were quickly cooled from a high temperature to the melting point of the intercalate (which strongly reduces the probability of forming a stable superlattice[8]) showed that the frequency spectrum of the oscillations does not depend on the rate of cooling. A partial deintercalation of the samples by exposure to air led to a decrease in oscillation frequencies with almost no change in amplitude; this should not occur in the case of formation of an ICl superlattice, the period of which cannot freely change.

Thus we can assume that the reason for the appearance of several isoenergetic surfaces in the hetero-IGCs is their rather complicated energy spectrum. One of the reasons for the complicated spectrum of the first-stage IGCs may be interaction between carbon atoms in neighboring layers separated by an intercalate layer. Such interaction clearly exists in donor IGCs.[10-13] There are in addition data [1,14,16] indicating the importance of interlayer interaction of carbon atoms in several acceptor-type IGCs. Therefore it is interesting to look at the consequences of this interaction in IGCs.

If we consider first-stage intercalated compounds to be an assembly of grapite layers, with an interlayer spacing somewhat larger than that in graphite, in which the role of the intercalate is only to change the carrier concentration in the layers, the interlayer interaction is naturally completely unimportant. In fact, the direct interaction between carbon atoms in neighboring layers, described in graphite by the parameter γ_1, is very sensitive to the interlayer distance and dies out exponentially as it is increased. Therefore, if in graphite with an interlayer distance $d_0 = 3.35$ Å the value of $\gamma_1 = 0.39$ eV, an order of magnitude less than the interlayer carbon atom interaction, then for an interlayer distance $d_i = 7.12$ Å (in the ICl IGC) the parameter γ_1 should be negligibly small. However, such a picture of intercalated compounds is evidently incorrect. The presence of intercalate molecules creates the possibility of indirect interaction between carbon atoms separated by intercalate molecules, by means of overlap between the acceptor and carbon $2p_z$ orbitals. Upon intercalation, then, the following would take place: direct interaction between carbon atoms would decrease, carrier concentrations within layers would change, and at the same time an additional indirect interaction would arise between carbon atoms in neighboring layers separated by an intercalate layer. Therefore, it is not possible,

strictly speaking, to neglect interlayer interactions and consider the intercalated graphite compounds as purely two-dimensional systems, in spite of the significant increase in interlayer distance.

In considering interlayer interactions we will start from the assumption that as an initial model we can use the McClure-Slonczewski-Weiss[17,18] model for graphite, with a modified set of parameters. Recall the carbon atoms in graphite are arranged in parallel layers, and in each planar layer there is a network of regular hexagons. This network is displaced from layer to layer (see Fig. 1a). This alternating-layer packing order is expressed as $ABAB$.

The McClure-Slonczewski-Weiss model uses seven parameters $(\Delta, \gamma_i, i = 0,1...5)$ to describe the graphite π-band near the hexagonal Brillouin-zone edge. These are usually determined from experimental data. They have the following physical interpretation: γ_0 is the nearest neighbor binding energy of carbon atoms in a layer; γ_1, γ_3, and γ_4 are determined by the wave-function overlap of carbon atoms of type AA, BB, and AB, respectively, in neighboring layers; γ_2 is connected with interaction of type b carbon atoms across a layer and mainly characterizes the band overlap; γ_5 is the interaction energy for atoms of type A across a layer; Δ is a parameter describing the inequivalence of atoms of types A and B in a layer. If we neglect the anisotropy of the band structure in the layer plane, that is, set $\gamma_3 = 0$, then the corresponding dispersion relation for the charge carriers has the form:

$$\varepsilon_e^{1,2} = \frac{E_{1,2}-E_3}{2} + \left[\left(\frac{E_{1,2}-E_3}{2}\right)^2 + \eta^2(1\mp v)^2 k_\rho^2\right]^{1/2}, \quad (1)$$

$$\varepsilon_h^{1,2} = \frac{E_{1,2}+E_3}{2} - \left[\left(\frac{E_{1,2}+E_3}{2}\right)^2 + \eta^2(1\mp v)^2 k_\rho^2\right]^{1/2}. \quad (2)$$

The first two equations pertain to the electron bands, the second, to the holes. In them, $E_{1,2} = \Delta \pm 2\gamma_1\cos\phi + 2\gamma_5\cos^2\phi$, $E_3 = 2\gamma_2^2\cos^2\phi$, $\phi = k_z c_0/2$, $\eta = 3\frac{1}{2}a_0\gamma_0/2$ and $v = (2\gamma_4/\gamma_0)\cos\phi$; k_ρ is the in-plane vector with components $(k_x, k_y, 0)$, and k_z is parallel to the c-axis. The vectors of the unit cell in the layer plane and along the c-axis are $a_0 = 2.46$ Å and $c_0 = 6.7$ Å, respectively. The parameters characterizing the graphite band structure are, in accordance with Ref. 19, $\Delta = -0.008$ eV, $\gamma_0 = 3.16$ eV, $\gamma_1 = 0.39$ eV, $\gamma_2 = -0.019$ eV, $\gamma_4 = 0.044$ eV, and $\gamma_5 = 0.038$ eV.

For the calculation of the energy spectrum in the model of Refs. 17, 18 a specific symmetry was assumed for the crystalline lattice and the electronic wave functions. In the hetero-IGCs the symmetry, in general, is different. However, in the first approximation we can consider the IGC energy spectrum to be given by the graphite spectrum, but with a parameter γ_1^* in the IGCs which describes the interaction of carbon atoms in neighboring layer separated by an intercalate layer. The parameter γ_1^* in the first-stage IGC takes into account the interaction of carbon atoms through an intercalate molecule; it can substantially differ therefore from its analog γ_1 in graphite. A similar remark applies to the parameter $\gamma_2(\gamma_5)$ of graphite, describing the interaction of atoms of type A (B) across a layer. Parameter γ_2^*, describing interaction of type A atoms in neighboring layer of first-stage IGCs (for the layer sequence AIA), but allowing for their interaction through an intercalate molecule, can likewise be

different from the graphite γ_2 and even exceed it, as in the AIA structure γ_2^* is the analog of γ_1.

In calculating the parameters characterizing the IGC energy spectrum, it is necessary first of all to analyze how stable the results are to variations in model parameters. Consider the role of Δ and γ_4 in the construction of the graphite energy spectrum. These parameters are substantially smaller than γ_0 and γ_1. A comparison of calcuational results for the Fermi energy, Fermi-surface cross-section and cyclotron mass, carried out using both the graphite values for Δ and γ_4 and assuming $\Delta = \gamma_4 = 0$, shows that calculated values in both cases differ by less than 3%.

Determinination of values of Δ and γ_4 from experimental values of the extremal Fermi-surface cross-section and the cyclotron mass is not possible. In further calculation of the hetero-IGC spectra we can (to the above limits of accuracy) take these parameters to be zero.

Assuming a layer sequence AIB for the IGC $C_{10}CuCl_2 \cdot 0.6$ ICl, and neglecting carbon-atom interactions across two intercalate layers and a carbon layer $(\gamma_2^* = \gamma_5^* = 0)$ we get from Eq. (1) a dispersion relation for two bands:

$$\varepsilon_{1,2} = \pm\gamma_1^*\cos\phi^* - (\gamma_1^{*2}\cos^2\phi^* + \eta^{*2}k_\rho^2)^{1/2}, \quad (3)$$

where $\phi^* = k_z I_c/2$, I_c is the repeat period of the IGC along the c-axis, and $\eta^* = 3^{1/2}a_0\gamma_0^*/2$. The two branches of the spectrum described by Eq. (3) are shown in Fig. 4. The value of the extremal cross section $S_{1,2}^K = \pi k_\rho^2$ in the $k_z = 0$ plane perpendicular to the c-axis is equal to

$$S_{1,2}^K = \frac{\pi|\varepsilon_F|(|\varepsilon_F|\pm 2\gamma_1^*)}{\eta^{*2}} \quad (4)$$

for the dispersion relation (3).

Using Eq. (4) we can find an expression for the carrier effective masses $m^*_{1,2} = (\hbar^2/2\pi)(\partial S/\partial E)$:

$$m^*_{1,2} = \frac{4\hbar^2}{3a_0^2\gamma_0^{*2}}(|\varepsilon_F|\pm\gamma_1^*). \quad (5)$$

The energy spectrum (3) thus leads to a Fermi surface in the shape of two undulating coaxial cylinders oriented along the c-axis, coming into contact at the Brillouin-zone boundaries $(k_z = \pm\pi/I_c)$ at the H-point. The degeneracy is removed via the theorem on non-intersection of levels. As
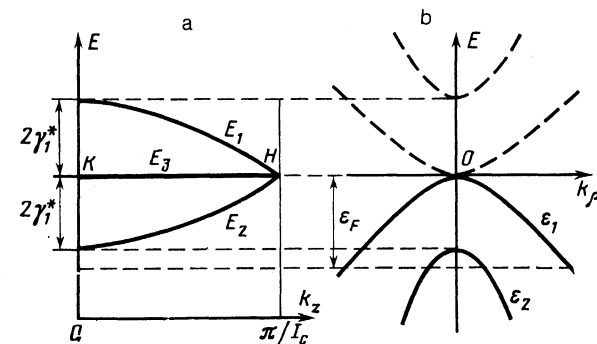

FIG. 4. The energy spectrum of the hetero-IGC $C_{10}CuCl_2 \cdot 0.6$ ICl: (a) energy levels along the KH direction in the Brillouin zone; $E_{1,2} = \pm 2\gamma_1^*\cos\phi$ and $E_3 = 2\gamma_2^*\cos^2\phi$; (b) dependence of energy on wave vector k_ρ for $\phi = 0$.
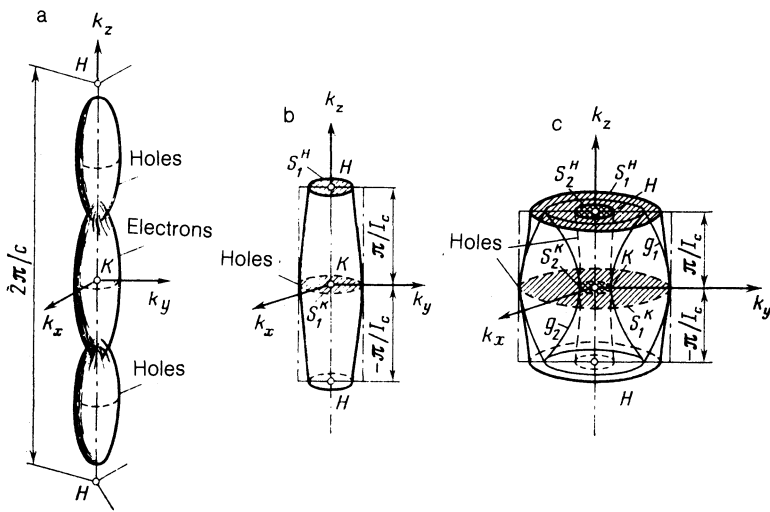
FIG. 5. The Fermi surface of the different IGCs and of graphite: (a) graphite (intrinsic carriers); (b) the second-stage IGC $C_{10}CuCl_2$; S_1^K and S_1^H are the extremal Fermi surface cross sections in the center (K point) and at the edge (H point) of the Brillouin zone; (c) the first-stage IGC $C_{10}CuCl_2 \cdot 0.6$ ICl; S_1^K and S_2^K are the extremal Fermi-surface cross section at the K-point, and S_1^H, S_2^H at the H-point. The lines g_1 and g_2 indicate the Fermi surface if degeneracy is not lifted at the Brillouin-zone edge.

a consequence of the lifting of degeneracy at the Brillouin zone edges two experimental Fermi-surface areas appear. In Fig. 5a the Fermi surface of graphite is shown, including the Brillouin zone edge; in Fig. 5b, the Fermi surface of the second-stage IGC of $C_{10}CuCl_2$, and in Fig. 5c, the Fermi surface of the first stage IGC of $C_{10}CuCl_2 \cdot 0.6$ ICl, with and without the removal of the degeneracy at the Brillouin zone boundary (the thin lines g_1 and g_2, and the thick lines, respectively). Thus, as a result of the heterointercalation, the original $C_{10}CuCl_2$ IGC Fermi surface, a smooth (or slightly undulating) cylinder is transformed into a Fermi surface consisting of two undulating coaxial cylinders along the c-axis, with two extremal cross sections S_1^K, S_2^K in the center of the Brillouin zone (the K point) and S_1^H, S_2^H at the Brillouin zone boundary (H point). The size of the undulation is (S_1^K - S_1^H)/$S_1^K \approx 2\%$ for the exterior cylinder and (S_2^H-S_2^K)/$S_2^H \approx 9\%$ for the internal one.

Using the experimental values for the Fermi surface cross section and the cyclotron mass, one can find using Eqs. (3)–(5) the spectral parameters $\varepsilon_F = -0.56$ eV, $\gamma_0^* = 2.0$ eV, and $\gamma_1^* = 0.27$ eV.

THE ShdH EFFECT AND THE ENERGY SPECTRUM OF THE FIRST-STAGE HETERO-IGC $C_{15}CuCl_2 \cdot 1.2$ ICl

The conductivity σ of the $C_{15}CuCl_2 \cdot 1.2$ ICl hetero-IGC is $\sim 1.8 \times 10^5$ ohm^{-1} cm^{-1} at room temperature and grows by a factor of 3–5 as the temperature is reduced to 4.2 K. In Fig. 6 are shown characteristic oscillations for the third-stage $C_{15}CuCl_2$ and for the same sample after additional introduction of iodine monochloride and formation of first-stage $C_{15}CuCl_2 \cdot 1.2$ ICl. In the Fourier spectra of the original and heterointercalated compounds three distinct peaks dominate. The positions of these peaks vary over a small range in the four measured samples, intercalated under exactly the same conditions. The presence of three different oscillation frequencies shows that the Fermi surface in these compounds consists of three coaxial cyclinders. The complex nature of the oscillation curves (the presence of a harmonic and difference frequencies) unfortunately does not permit any kind of conclusions on the degree of their undulation.

The existence of several isoenergetic surfaces in the

$C_{15}CuCl_2 \cdot 1.2$ ICl IGC spectrum can be explained if we assume that the complex structure of this compound can be thought of in first approximation as an aggregate of two types of stacks of layers: a stack in which the layer alternation AIB is like that in the $C_{10}CuCl_2 \cdot 0.6$ ICl IGC, and a stack with a different sequence AIA of layers. To describe the energy spectrum of the first type of stack we can use the model described above, taking into account that the parameters can now have different values. This is because the structure of $C_{15}CuCl_2 \cdot 1.2$ ICl is different from that of the $C_{10}CuCl_2 \cdot 0.6$ ICl compound. Therefore, the existence of AIB regions leads to the creation of two branches $\varepsilon_{1,2}$ in the energy spectrum, described by Eq. (3) with altered parameters. To determine these parameters we make use of Eq. (4) with the new experimentally determined values of $S_{1,2}$. This leads to the values $\gamma_0^* = 2.4$ eV and $\gamma_1^* = 0.28$ eV.

We find a representation of the spectrum of the AIA stack of layers by the following reasoning. Let us use the graphite structure as a starting point. The interaction between AA atoms across the displaced layer B is described by the γ_2 parameter. In the AIA stack an intercalate layer is in place of the graphite B layer. As was shown above, the presence of an intercalate layer can substantially change γ_2 from
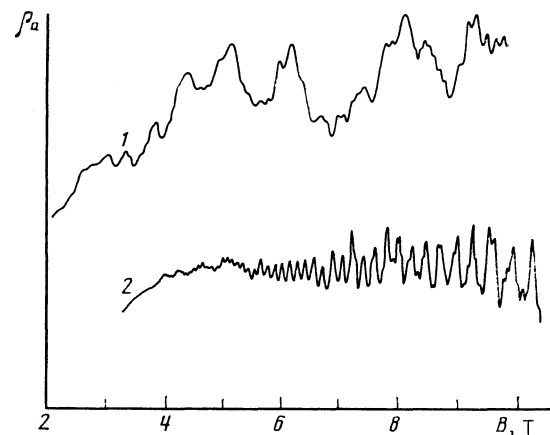

Fig. 6. Dependence of the oscillatory part of the transverse magnetoresistance ρ_a on magnetic field; 1—the third-stage IGC $C_{15}CuCl_2$; 2—the first-stage hetero-IGC $C_{15}CuCl_2 \cdot 1.2$ ICl.
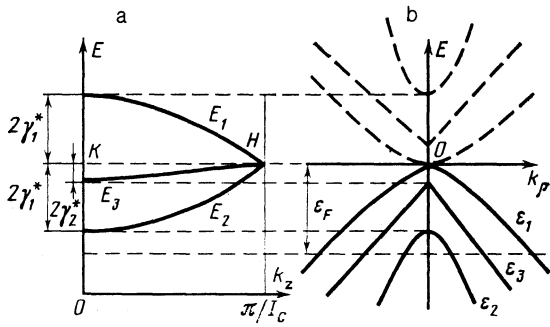
FIG. 7. The energy spectrum of the IGC $C_{15}CuCl_2 \cdot 1.2$ ICl: (a) energy levels along the KH direction in the Brillouin zone; $E_{1,2} = \pm 2\gamma_1^* \cos\phi$, $E_3 = 2\gamma_2^* \cos^2\phi$; (b) energy dependence on the wave vector K_ρ for $\phi = 0$.

its value in graphite. We will denote this parameter in the IGC by γ_2^*. Let us consider that for the AIA structure parameter γ_1 is zero, and $\gamma_2^* = \gamma_3^*$. Then to describe the new energy subband, arising from the AIA layer stack, we can utilize Eq. (2). Putting in (2) $\gamma_1 = 0$, $\gamma_2 = \gamma_5$ and changing γ_2 to γ_2^*, we find for the new energy subband the expression:

$$\varepsilon_3 = 2\gamma_2^* \cos^2 \phi - \eta^* k_\rho. \qquad (6)$$

Thus, a composite structure of the type AIA and AIB leads in first approximation to a three-band structure (Fig. 7) described by the relationships (3) and (6). For such a spectrum the Fermi surface consists of three undulating coaxial cylinders along the c-axis. The size of the third extremal Fermi surface cross-section at the center of Brillouin zone, $S_3^K = \pi k_\rho^2$, is

$$S_3^K = \frac{\pi (|\varepsilon_F| + 2\gamma_2^*)^2}{\eta^{*2}} \qquad (7)$$

and the effective mass $m_3^* = (\hbar^2/2\pi)(\partial S_3^K/\partial\varepsilon)$ is:

$$m_3^* = \frac{4\hbar^2}{3a_0^2\gamma_0^{*2}} (|\varepsilon_F| + 2\gamma_2^*). \qquad (8)$$

Using the experimentally determined value of the Fermi surface cross section, we get from (7) $\gamma_2^* = -0.11$ eV. For the found values of γ_0^*, γ_1^* and γ_2^* the value of ε_F is -0.69 eV. We note that the value of γ_0^* for the IGCs investigated decreases as hole concentration increases (see Table II). The decrease of γ_0^* can be linked to the fact that as the hole concentration increases, the screening radius decreases. However, it must be kept in mind that the value of γ_0^* is calculated based on an assumed simplified model for describing the energy spectrum of the hetero-IGCs. Therefore the absolute values of the parameters may be somewhat too low; but the tendency of γ_0^* to decrease with growth in the carrier concentration is correctly represented.

ORDER-DISORDER PHASE TRANSITIONS

It is known that when IGCs are cooled to a certain temperature a phase transition occurs due to the solidification of the intercalate layer. Depending on the size and type of introduced molecules, and also on the cooling rate, the fluid intercalate layer may transform to an ordered crystalline or amorphous solid layer. In the first case a disorder-order type phase transition occurs, accompanied by a significantly stronger change in IGC properties than for formation of an amorphous intercalate layer. In the mono-IGCs of iodine monochloride disorder-order transitions occur for $T_{cr} = 308$–317 K (T_{cr} grows as the IGC stage number increases) and is easily registered by the discontinuity in resistivity ρ_c along the c-axis. It is of interest to investigate the details of ordering for phase transitions in the hetero-IGCs.

In Fig. 8 the relative change in c-axis resistivity

$$\Delta\rho_c/\rho_c(295) = [\rho_c(T) - \rho_c(295)]/\rho_c(295) \qquad (9)$$

is shown for the hetero-IGCs $C_{10}CuCl_2 \cdot 0.6$ ICl (curve 1), $C_{15}CuCl_2 \cdot 1.2$ ICl (curve 2) and the first-stage IGC C_8ICl (curve 3). All three compounds are first-stage IGCs, although the transition in $C_{10}CuCl_2 \cdot 0.6$ ICl occurs at a lower temperature than in the C_8ICl IGC. Since in the compound $C_{10}CuCl_2 \cdot 0.6$ ICl half of the ICl layers are changed to $CuCl_2$ (see Fig. 1b), the temperature shift of the transition means that a change of an ICl layer to a $CuCl_2$ leads to a reduced interaction in the remaining ICl layers. Note that the resistivity discontinuity for the transition in the hetero-IGC $C_{10}CuCl_2 \cdot 0.6$ ICl is less by a factor of 2. The resistivity variation for the phase transition in the hetero-IGC $C_{15}CuCl_2 \cdot 1.2$ ICl, in which (in contrast to the previous compound) only a third of the ICl layers are changed to $CuCl_2$, has three rather pronounced regions. The first and the last almost coincide with the temperatures of the phase transitions in the C_8ICl IGC and the hetero-IGC $C_{10}CuCl_2 \cdot 0.6$ ICl, which evidently indicates the presence of grain boundaries in the $C_{15}CuCl_2 \cdot 1.2$ ICl layer structure having the structure characteristic of the C_8ICl and $C_{10}CuCl_2 \cdot 0.6$ ICl IGCs. As for the central part of the transition, the resistivity change in this temperature region can be ascribed to the presence of defect clusters of complex structure.

PRESSURE DEPENDENCE OF THE ENERGY SPECTRUM OF THE HETERO-IGC $C_{10}CuCl_2 \cdot 0.6$ ICl

Pressure was applied in a beryllium bronze cell at room temperature in a pentane oil medium, wih subsequent cooling to helium temperature. During the cooling process the pressure fell to ~ 3.5 kbar due to the difference in thermal expansion coefficients between the pressure-transmitting medium and the cell material. A rise in the hydrostatic character of the pressure caused sample warming during the cooling process.
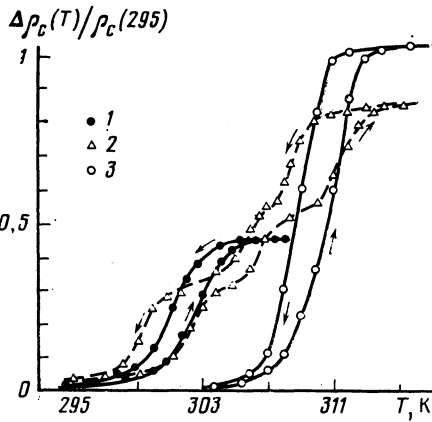
TABLE II. Correlation of the γ_0^* parameter and hole concentration n_p.

Состав СВГ	$C_{10}CuCl_2$	$C_{16}ICl$	$C_{28}ICl_3$	$C_{10}CuCl_2 \cdot 0,6ICl$	$C_{15}CuCl_2 \cdot 1,2ICl$
N	2	2	2	1	1
$n_p \cdot 10^{20}$, cm^{-3}	1,3	2,5	2,9	6,5	2,1
γ_0^*, eV	2,7	2,7	2,6	2,0	2,4

FIG. 8. Relative change in resistivity ρ_c along the c-axis in first-stage IGCs: 1—$C_{10}CuCl_2 \cdot 0.6$ ICl; 2—$C_{15}CuCl_2 \cdot 1.2$ ICl; 3—C_8ICl.

FIG. 10. Dependence of the relative change in extremal Fermi-surface cross sections in the hetero-IGC $C_{10}CuCl_2 \cdot 0.6$ ICl under pressure at 4.2 K. Different symbols for data points refer to different samples.

In Fig. 9 we plot the dependence of the oscillating part of the resistivity ρ_a in the basal plane on magnetic field B perpendicular to the plane at 4.2 K, for different pressures. Under pressure the high frequency (Fermi surface cross section S_1^K) increases at the rate $\partial \ln S_1^K/\partial p \approx 0.03$ kbar^{-1}. The corresponding oscillation amplitude quickly decreases, so that for $p \gtrsim 2$ kbar in fields $B \lesssim 8.5$ T the oscillations are almost not observed. We note that without an increase in the hydrostatic character of the cell pressure the oscillations from S_1^K are not seen as a general rule. The smaller Fermi-surface cross-section S_2^K also grows with compression, but its rate of change $\partial \ln S_2^K/\partial p \approx 0.14$ kbar^{-1} is significantly greater than that of S_1^K (Fig. 10). A new ShdH oscillation frequency appears for pressure $p \gtrsim 1$ kbar, corresponding to a cross section $S_2 = 264 \times 10^{-12}$ cm^{-2} characteristic of the second-stage IGC $C_{16}ICl$. The cross section S_2 decreases with compression.

For pressures over 5 kbar, irreversible changes in sample structure set in, accompanied by a sharp fall in oscillation amplitudes corresponding to the heterostructure (the cross sections S_1^K and S_2^K). At the same time, a new frequency appears, typical of second-stage $C_{10}CuCl_2$. Thus, the hetero-structure investigated seems to be stable only in certain regions of pressure. In spite of the fact that the second-stage $C_{16}ICl$ regions appear at pressures for which the hetero-structure maintains stability and for which the pressure dependence of cross sections S_1^K and S_2^K is almost completely
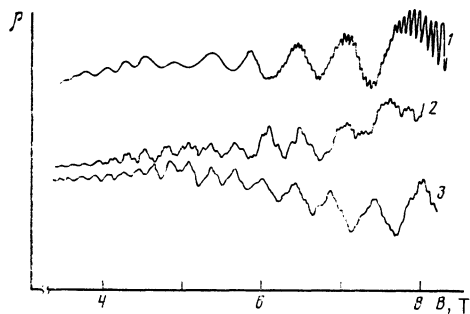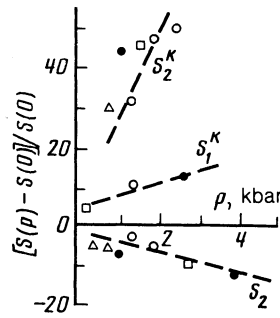

FIG. 9. The oscillatory part of the transverse magnetoresistance in the basal plane, ρ_a, in the hetero-IGC $C_{10}CuCl_2 \cdot 0.6$ ICl for different pressures p: 1—0.001 kbar; 2—1.3 kbar; 3—2.6 kbar.

reversible, the formation mechanism for these regions is unclear. One possibility in formation of the second-stage regions is the displacement of ICl molecules at domain boundaries which exist in the $C_{10}CuCl_2 \cdot 0.6$ ICl hetero-IGC. However, such a process is only possible if the original sample has less than the maximal $CuCl_2$ content.

Using expression (4) for the external Fermi-surface cross section, it is possible to calculate the change in energy-spectrum parameters in $C_{10}CuCl_2 \cdot 0.6$ ICl under pressure within the model assumed. The parameter γ_0^*, which characterizes carbon atom interactions in a layer, changes insignificantly compared to the parameters for interlayer interaction, and therefore to first approximation we can take $\partial\gamma_0^*/\partial p = 0$. Then Eq. (4) yields the relations

$$\frac{\partial \ln S_1^K}{\partial p} = \left(1 + \frac{|\varepsilon_F|}{|\varepsilon_F| + 2\gamma_1^*}\right)\frac{\partial \ln |\varepsilon_F|}{\partial p} + \frac{2\gamma_1^*}{|\varepsilon_F| + 2\gamma_1^*}\frac{\partial \ln \gamma_1^*}{\partial p},$$

$$\frac{\partial \ln S_2^K}{\partial p} = \left(1 + \frac{|\varepsilon_F|}{|\varepsilon_F| - 2\gamma_1^*}\right)\frac{\partial \ln |\varepsilon_F|}{\partial p} - \frac{2\gamma_1^*}{|\varepsilon_F| - 2\gamma_1^*}\frac{\partial \ln \gamma_1^*}{\partial p},$$

(10)

which determine the rate of change of the S_1^K and S_2^K cross sections under pressure. Using the experimental values for the derivatives on the left-hand side, we find the pressure dependence of the Fermi energy and the γ_1^* parameter to be given by: $\partial\varepsilon_F/\partial p = 12$ meV/kbar, $\partial \ln|\varepsilon_F|/\partial p \approx 0.022$ kbar^{-1}, and $\partial \ln\gamma_1^*/\partial p = 0.01$ kbar^{-1}.

The variation in cyclotron masses under pressure, based on Eq. (5), is described by

$$\frac{\partial \ln m_{1,2}^*}{\partial p} = (|\varepsilon_F| \pm \gamma_1^*)^{-1}\left(|\varepsilon_F|\frac{\partial \ln|\varepsilon_F|}{\partial p} \pm \gamma_1^*\frac{\partial \ln \gamma_1^*}{\partial p}\right).$$

(11)

Substituting in (11) the values of $\partial \ln|\varepsilon_F|/\partial p$ and $\partial \ln \gamma_1^*/\partial p$, we get $\partial \ln m_1^*/\partial p \approx 0.01$ kbar^{-1} and $\partial \ln m_2^*/\partial p \approx 0.018$ kbar^{-1}. This last value agrees well with the value $\partial \ln m_2^*/\partial p = 0.015$ kbar^{-1} obtained from the temperature dependence of the oscillation amplitudes.

In conclusion we would like to direct attention to the following important fact. One of the basic questions of the physics of the IGCs deals with the nature of the interactions between intercalate molecules and carbon atoms; up to now this does not have an unambiguous solution. It is possible to describe the energy spectrum of different intercalated compounds of graphite using the McClure-Slonczewski-Weiss

model proposed for graphite, with adjustable parameters, a minimal set of which is determined by the symmetry characteristic of the IGC studied. This indicates that a fundamental role in the formation of the IGC spectrum is played by the graphite energy spectrum and the symmetry of the graphite matrix (if the intercalate molecules do not form a superlattice). The function of the intercalate is not only to change the carrier concentrations in the graphite layers, but also to enable indirect interactions between layers of graphite separated by an intercalate layer.

We would like to acknowledge useful discussions of our results with J. McClure.

[1] M. S. Dresselhaus and G. Dresselhaus, Adv. Phys. **30**, 139 (1981).
[2] M. Suzuki, P. C. Chow, and H. Zabel, Phys. Rev. B **32**, 6800 (1985).
[3] V. Ya. Akim, V. H. Davydov, V. A. Kulbachinskii, and O. M. Nikitina, Pis'ma v Zh. Eksp. Teor. Fiz. **45**, 567 (1987) [JETP Lett. **45**, 724 (1987)].
[4] A. Herold, G. Furdin, D. Guerard, et al., Ann. de Phys., Coll. 2, Suppl. 2, **11**, 3 (1986).
[5] M. Heerschap, P. Delavignette, and S. Amelinchx, Carbon **1**, 235 (1964).
[6] J. Blinowski, Nguen Hy Hay, C. Rigaux, and J. P. Vieren, J. de Phys. **4**, 47 (1980).
[7] D. Ghosh, R. Gangwar, and D. D. L. Chung, Carbon **22**, 325 (1984).
[8] Y. Yosida and S. Tanuma, J. Phys. Soc. Jpn. **54**, 701 (1985).
[9] F. Batallan, I. Rosenman, C. Simon, et al., Physica B **99**, 411 (1980).
[10] S. Y. Leung and G. Dresselhaus, Phys. Rev. B **24**, 3490 (1980).
[11] G. Dresselhaus and S. Y. Leung, Solid State Commun. **35**, 819 (1980).
[12] G. Dresselhaus and S. Y. Leung, Physica B **105**, 495 (1981).
[13] R. C. Tatar and S. Rabii, Phys. Rev. B **25**, 4126 (1981).
[14] Y. Iye, O. Takahashi, S. Tanuma, et al., J. Phys. Soc. Jpn. **51**, 475 (1982).
[15] S. Tanuma, Physica B **105**, 486 (1981).
[16] R. S. Markiewicz, Solid State Commun. **57**, 237 (1986).
[17] J. W. McClure, Phys. Rev. **108**, 612 (1957).
[18] J. W. Slonczewski and P. R. Weiss, Phys. Rev. **109**, 272 (1958).
[19] E. Mendez, A. Misu, and M. S. Dresselhaus, Phys. Rev. B **21**, 827 (1980).

Translated by I. A. Howard